DOI: 10.1002/ejic.200701012

Structural Effects of Codoping of Nb and Sc in Titanium Dioxide Nanoparticles

Akhlaq Ahmad,*[a] Jawad Ali Shah,[a] Scott Buzby,[b] and Syed Ismat Shah[b,c]

Keywords: TiO_2 / Nanostructures / Sol–gel processes / Calcination / Niobium / Scandium

Nanoparticles of TiO_2 codoped with 0.5, 0.75, and 1 atom-% Nb and Sc each were synthesized by sol–gel technique. After drying, as-synthesized samples were calcined at temperatures ranging from 250–900 °C. Changes in phase transformation of the doped samples with reference to dopant concentration and calcination temperature have been studied. The samples were analyzed by various analytical tools such as XRD, SEM, TEM, XPS, and EDS. The XRD results indicate that the presence of Nb and Sc substitutional ions in the anatase crystal structure inhibits the phase transition and growth of the nanoparticles with an increase in temperature. The XPS results indicate the incorporation of Nb as Nb_2O_5 and Sc as Sc_2O_3.

Introduction

Titanium dioxide is a ceramic material commonly known as titania. During the past two decades, it has received great attention by materials scientists, physicists, and environmental engineers because of its chemical stability, lack of toxicity, and its potential utility for the total destruction of most of the organic compounds in polluted air and waste water.[1,2] It is capable of decomposing a wide variety of organic and inorganic pollutants such as DDT, dichloronitrobenzene, trichloroethylene, H_2S, NO, and Cr^{IV}.[3,4] However, the bandgap (E_g) of TiO_2 anatase is ≈ 3.2 eV[5], which lies in the UV range so that only 5–8% of sunlight photons have the required energy to activate the catalyst. This relatively large bandgap has significantly limited more widespread applications, particularly for situations indoors.

An effective way of improving TiO_2 photocatalytic activity is to introduce foreign metal ions into TiO_2.[6–8] This enhancement in photocatalytic activity is due to the formation of shallow charge trapping sites on the surface of the TiO_2 nanoparticles as a result of replacement of Ti^{4+} by metal ions. Doping of the TiO_2 lattice with metal ions introduces new energy levels in the bandgap. Depending on the dopant type and concentration, the bandgap of TiO_2 can be tailored to extend the photoresponsiveness into the visible light region.

Numerous workers employed the sol–gel route to introduce dopants such as Co^{2+},[7] Nd^{3+},[6] Cu^{2+},[9] Fe^{3+},[10] V^{5+},[11] and Zn^{2+}[10] into TiO_2 powders and films. In their published work, these researchers reported an improvement in the photocatalytic activity of doped TiO_2 to varying extents. The dopants introduced by the sol–gel method usually affect the TiO_2 phase transformation behavior and structure. It is therefore interesting and necessary to examine the effect of dopants on the TiO_2 phase transformation and grain growth before their application.

Among the three crystal structures of TiO_2, anatase, as a result of its higher photocatalytic activity, is commonly used for photocatalysis, membranes, and sensors.[12,13] One of the problems in the application of anatase-based materials both in catalysis and as sensors is its transformation to rutile. This transformation is dependent on several parameters such as initial particle size, initial phase, dopant concentration, reaction atmosphere, and annealing temperature.[6,14]

It has been reported that doping of TiO_2 with non-isovalent cations may improve the catalytic activity of TiO_2 particles. Nanoparticles of TiO_2 that are synthesized and codoped with Sc^{3+} and V^{5+} ions by the sol–gel method have been reported by Dong et al.[15] In the present study, we synthesized nanoparticles of TiO_2 codoped with Sc^{3+} and Nb^{5+} by the sol–gel method. These nanoparticles were calcined at various temperatures. The effect of codoping on the stability of the anatase phase was investigated. Sc and Nb are p-type and n-type dopants, respectively. The effect of the addition of Nb only has already been reported by the authors in a separate paper.[16] The simultaneous addition of Sc^{3+} and Nb^{5+} ions may improve the photocatalytic activity of the nanosized particles.

[a] Department of Metallurgical and Materials Engineering, University of Engineering and Technology,
Lahore, Pakistan
Fax: +92-429250202
E-mail: aamalik87@fulbrightweb.org
[b] Department of Materials Science and Engineering, University of Delaware, Newark, DE 19716, USA
[c] Department of Physics and Astronomy, University of Delaware, Newark, DE 19716, USA

Results and Discussion

Figure 1 shows the XRD pattern of as-synthesized TiO_2 doped with 0.5 , 0.75, and 1.0 atom-% Nb and Sc each. As is evident, the particles are amorphous in nature. Figure 2 shows the XRD patterns of the TiO_2 sample doped with 0.5 atom-% Nb and Sc each and calcined at temperatures ranging from 250–850 °C. The particles calcined up to 300 °C are amorphous. Transformation to anatase, with the presence of a large amorphous band in the X-ray diffraction pattern, is evident at 350 °C. The first XRD peaks to appear are all from anatase. At low calcination temperatures, the XRD peaks of anatase are weak and broad. As the calcination temperature is increased, the intensity of anatase band increases and the peaks sharpen, which indicates improved crystallinity. Pure anatase persists up to 650 °C. The anatase peaks are indexed as (101), (004), (200), (105), (211), (204), and (215), in the order of increasing diffraction angles, which indicates a body-centered tetragonal crystalline structure for the TiO_2 crystal. The peaks are broad at low calcination temperatures, which indicates a small TiO_2 nanocrystalline particle size. Transformation from anatase to rutile begins to take place at temperatures above 650 °C. The intensity of the anatase phase decreases and the intensity of the rutile phase increases with increasing calcination temperature. Figure 2 shows that peaks related to rutile become more evident and sharper as the calcination temperature is increased to above 700 °C. A mixture of both anatase and rutile phases is present up to a calcination temperature of 800 °C. No peaks for anatase were observed at or above 850 °C, which indicates complete phase transformation from anatase to rutile.

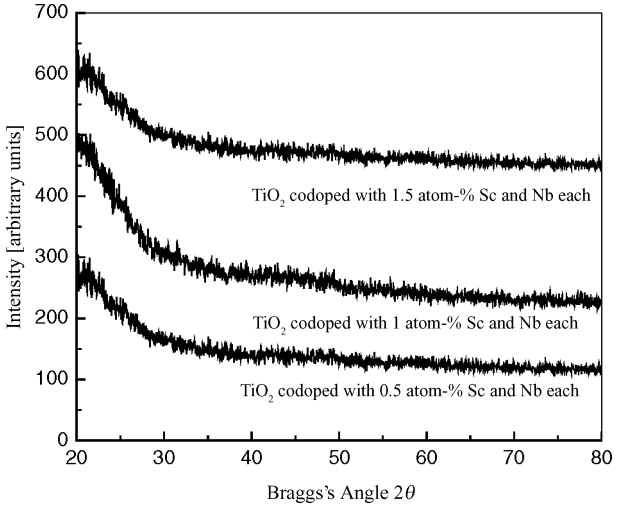

Figure 1. XRD patterns of as-synthesized TiO_2 nanoparticles codoped with Sc and Nb.

Figure 3 shows the XRD patterns of the nanostructured titania with different dopant concentration and with various calcination temperature. Table 1 presents the percentage of anatase and rutile with respect to the calcination temperature in the samples doped with 0.5, 0.75, and 1.0 atom-% Nb and Sc each. It is evident that both the dopant concentration and the calcination temperature influences the percentage of anatase and rutile phases present in the samples. By increasing the Nb and Sc content in the doped samples, the anatase phase is stabilized. For the sample doped with 0.5 atom-% Nb and Sc each, 76% and 21% anatase is present when this sample was calcined at 700 °C and 750 °C, respectively. For the sample doped with 0.75 atom-% Nb and Sc each, 100% and 83% anatase was present when the sample is calcined at 700 °C and 750 °C, respectively. For the sample doped with 1 atom-% Sc and Nb each, 100% and 98% anatase is present when this sample was calcined at 700 °C and 750 °C, respectively.

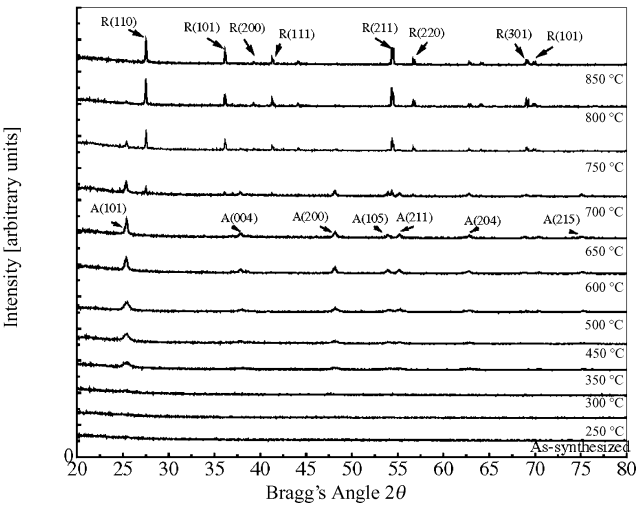

Figure 2. XRD patterns at different calcination temperatures for nanostructured titania codoped with 0.5 atom-% Sc and Nb each (A anatase; R rutile).

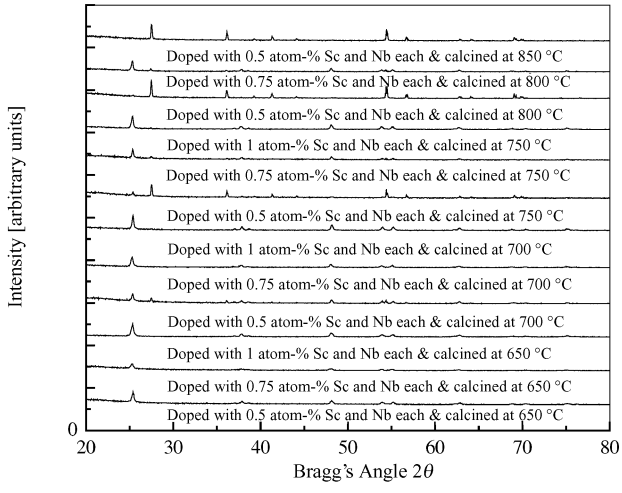

Figure 3. XRD patterns of the nanostructured titania with various dopant concentrations and calcination temperature.

Table 2 shows the anatase particle size of undoped and doped samples as determined by XRD. The anatase particle size of the doped and undoped samples increases with the

Table 1. Percentage of anatase and rutile phase with respect to the calcination temperature in the doped samples (as determined by XRD).

Doped TiO_2 sample	Heating temperature [°C]	Anatase TiO_2	Rutile TiO_2
0.5 atom-% Nb and Sc each	650	100	–
	700	76	24
	750	21	79
	800	03	97
	850	01	99
0.75 atom-% Nb and Sc each	650	100	–
	700	100	–
	750	83	17
	800	86	14
	850	–	–
1 atom-% Nb and Sc each	700	100	–
	750	98	2
	800	–	–
	850	–	–

increase in calcination temperature. However, the anatase grain growth is less in the doped samples than in the undoped samples. The results indicate that doping inhibits anatase grain growth, which in turn stabilizes the anatase phase and slows down the transformation from anatase to rutile.

Table 2. Anatase particle size of undoped and doped samples as determined by XRD (R indicates the rutile phase).

Sample	Calcination temperature [°C]	Particle size [nm]
Undoped TiO_2	500	17.5
	600	43.73
	650	47.7
	700	56.0, 82.2 (R)
TiO_2 doped with 0.5 atom-% Nb and Sc each	500	17.0
	600	29.22
	650	35.21
	700	44.34, 78.19 (R)
TiO_2 doped with 0.75 atom-% Nb and Sc each	500	18.4
	600	23.1
	650	29.3
	700	34.0
TiO_2 doped with 1 atom-% Nb and Sc each	500	18.7
	600	–
	650	31.6
	700	44.23

The atomic radii of Ti^{4+}, Nb^{5+}, and Sc^{3+} are 0.70 Å, 0.68 Å, and 0.745 Å, respectively.[13,15] The similarity in the atomic radii of Ti^{4+} and Nb^{5+} indicates that the solubility of Nb in TiO_2 phases will depend mainly on the charge compensation mechanism rather than on the induced stress. As proposed by Arbiol et al.,[13] the introduction of Nb should reduce the amount of oxygen vacancies because of the higher positive charge of Nb than that of Ti. When Nb ions enter substitutionally into TiO_2, the charge of the Nb^{5+} ions should be compensated for by a decrease in oxygen vacancies, which leads to the hindering of the growth of the anatase particles and of the transformation from anatase to rutile for the TiO_2 nanoparticles.

The atomic radii of Sc^{3+} (0.745 Å) is larger than that of Ti^{4+} (0.68 Å). Because of its large ionic radius, it is difficult for the Sc^{3+} ions to act as interstitial ions in the TiO_2 matrix. Therefore, the Sc^{3+} ion can only replace Ti^{4+} substitutionally in the lattice sites. The introduction of substitutional metal ions with a valency of less than 4 would induce oxygen vacancies at the surface of the anatase grains, which should favor ionic rearrangement and structure reorganization for the formation of the rutile phase, as observed for the Ag^{1+} ion.[4] However since the radius of Sc^{3+} is bigger than that of Ti^{4+}, it induces stress in the titania lattice, which may hinder the growth of TiO_2 crystallites to a certain extent. Therefore, increasing the simultaneous addition of Nb and Sc ions in the TiO_2 lattice from 0.5 atom-% each to 1.0 atom-% each, results in the inhibition of anatase grain growth and of the transformation from anatase to rutile.

Figure 4a and b show the TEM bright-field images of TiO_2 calcined at 500 °C and doped with 0.5 atom-% and 0.75 atom-% Nb and Sc each, respectively. As evident from the micrographs, well-defined, discrete, and irregular spherical nanoparticles are formed. The average grain size is below 20 nm in both samples. The particle sizes measured by TEM are generally in agreement with those determined by XRD, though some agglomeration is apparent because of the high surface energy of the nanoparticles. Furthermore, neither XRD nor the TEM results show the presence of any Nb or Sc clusters or Nb- or Sc-related second phase around the TiO_2 anatase nanoparticles. This is in agreement with the results reported by Dong et al.[16] in the samples co-doped with 2 atom-% Sc^{3+} and V^{5+} ions.

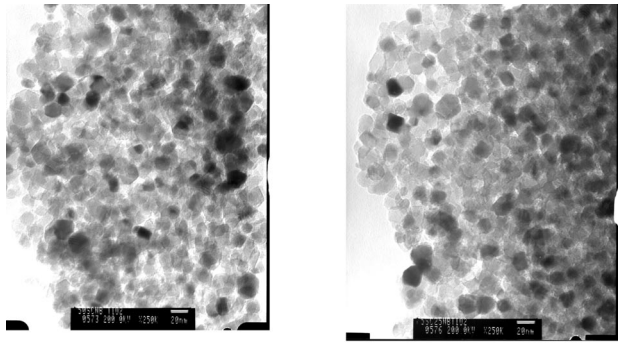

a) b)

Figure 4. TEM bright-field image of TiO_2 doped with (a) 0.5 atom-% Nb and Sc each; (b) 0.75 atom-% Sc and Nb each. Both samples are calcined at 500 °C.

Figure 5 shows the EDS result for TiO_2 codoped with 0.5 atom-% Nb and Sc each, calcined at 500 °C. The EDS results confirm the presence of the pure anatase phase at

this calcination temperature. Neither the XRD nor the TEM/EDS results show the presence of any Nb- or Sc-related second phase.

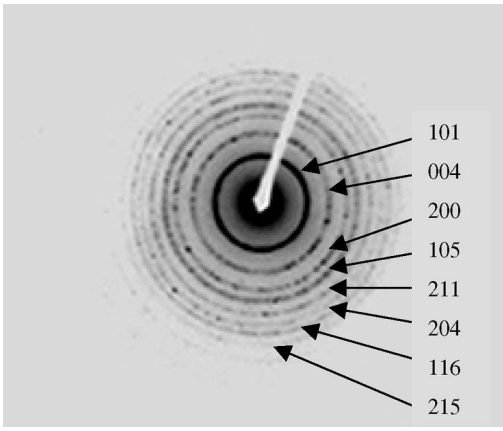

Figure 5. Electron diffraction pattern for anatase TiO_2 codoped with 0.5 atom-% Nb and Sc each, calcined at 500 °C.

The valency state and the Nb and Sc content in the doped sample calcined at 500 °C were determined by X-ray photoelectron spectroscopy and energy dispersive spectroscopy. The Nb and Sc concentrations measured by both techniques are similar and are close to the initial values used at the preparation step of the samples, which indicates that all the Sc or Nb is incorporated into TiO_2.

Figure 6 shows the XPS survey spectra of the sample doped with 1 atom-% Nb and Sc each. The survey scan from the sample confirms the content of niobium, scandium, titanium, oxygen, and carbon. No other contaminants are detected, except for the above-mentioned elements. A rough estimation of the Sc or Nb concentration from the XPS data matches well with that measured by EDS. Figure 7 shows the high-resolution XPS spectra of the Nb 3d region of the TiO_2 sample doped with 1 atom-% Nb and Sc each. Metallic Nb $3d_{5/2}$ and Nb $3d_{3/2}$ peaks occur at 202 and 205 eV, respectively. No such peaks were observed in the doped sample. Therefore, there is no evidence to suggest the presence of Nb metal clusters. This is in agreement with the XRD result that did not show the existence of any pure Nb phase. The reported value of the binding energy of Nb $3d_{5/2}$ in Nb_2O_5 is 207.5 eV, with a difference of 2.8 eV in the binding energy between the Nb $3d_{5/2}$ and Nb $3d_{3/2}$ peaks. As evident from Figure 7, the positions of the Nb $3d_{5/2}$ and Nb $3d_{3/2}$ peaks in our sample correspond to 206.2 and 208.7 eV, respectively, which is similar to the reported value. Nb is therefore incorporated within the TiO_2 lattice as Nb^{5+}. Our results are consistent with the conclusions derived by Sacerdoti et al.[17] and Arbiol et al.[13] in their separate studies on Nb-doped TiO_2 samples synthesized by the sol–gel method and laser-induced pyrolysis, respectively. The XPS study of Nb-doped TiO_2 samples by Moris et al.[18] also confirms that the oxidation state of Nb is 5+ for TiO_2 samples doped at low Nb concentrations.

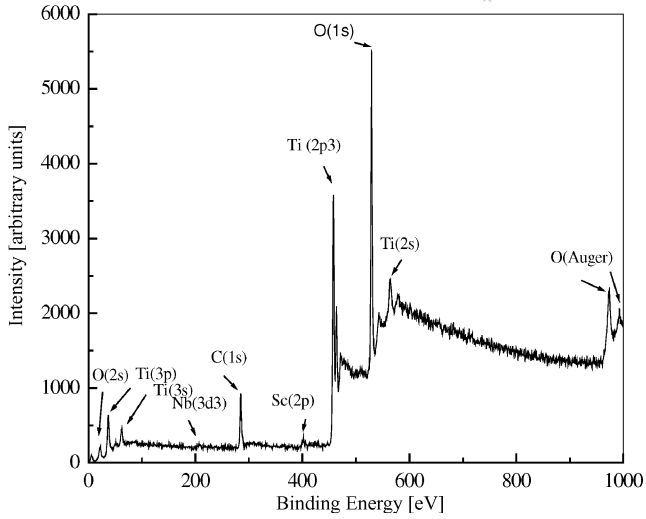

Figure 6. XPS survey spectra of the sample doped with 1 atom-% Nb and Sc each.

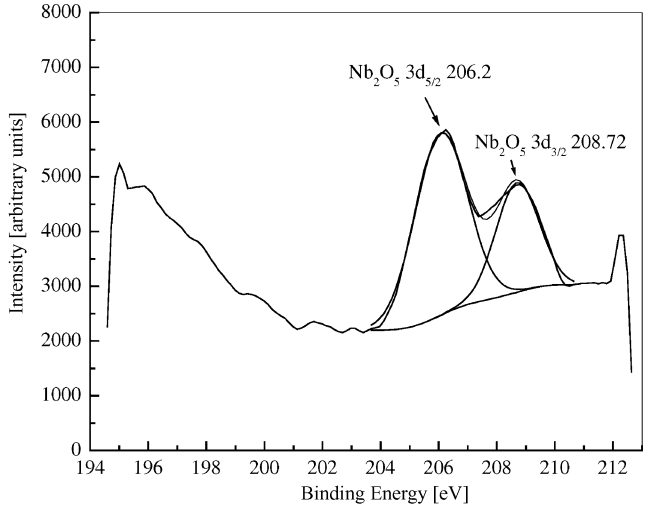

Figure 7. High-resolution XPS spectra of the 3d region of Nb in the TiO_2 sample doped with 1 atom-% Nb and Sc each.

Figure 8 shows the high resolution XPS spectra of the 2p region of Sc in TiO_2 doped with 1 atom-% Sc and Nb each. The metallic Sc $2p_{3/2}$ peak occurs at 398.7 eV.[18] No such peak was observed in the doped sample. This is in agreement with the XRD result that did not show the existence of any pure Sc phase. The reported values of the binding energy of Sc $2p_{3/2}$ and Sc $2p_{1/2}$ in Sc_2O_3 are 401.7 and 406 eV, respectively.[19] The measured values for our sample are 401.6 and 406 eV for Sc_2O_3 $2p_{3/2}$ and Sc_2O_3 $2p_{1/2}$, respectively. It is therefore concluded that Sc is incorporated into the TiO_2 lattice as Sc^{3+}.

Figure 9 shows a high-resolution XPS spectra of the 2p region of Ti in the TiO_2 sample doped with 1 atom-% Nb and Sc each. Two peaks located at 458.1 and 463.75 eV are identified for Ti $2p_{3/2}$ and $2p_{1/2}$, respectively. For metallic Ti, these two peaks are expected to be at 453.8 and 459.95 eV, respectively.[20] The shift in the Ti $2p_{3/2}$ and Ti $2p_{1/2}$ peak positions is similar to that observed by Burns et

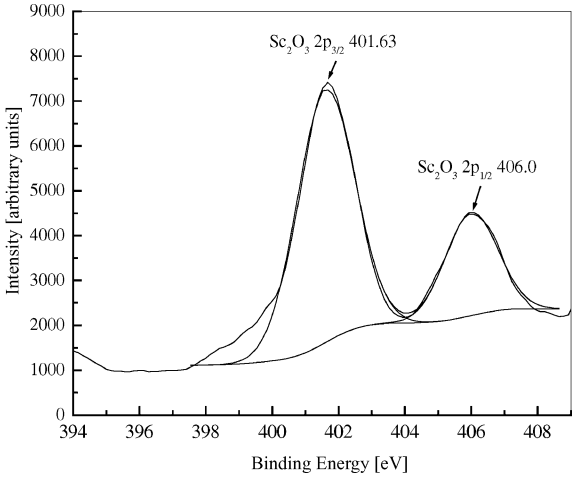

Figure 8. High-resolution XPS spectra of the 2p region of Sc in TiO_2 doped with 1 atom-% Sc and Nb each.

al.[20] for Nd-doped TiO_2. The peak shifts in the Ti $2p_{3/2}$ and Ti $2p_{1/2}$ peak positions and the change in the separation between these two peaks is caused by the presence of tetravalent Ti^{4+}, which is consistent with the formation of TiO_2.[20]

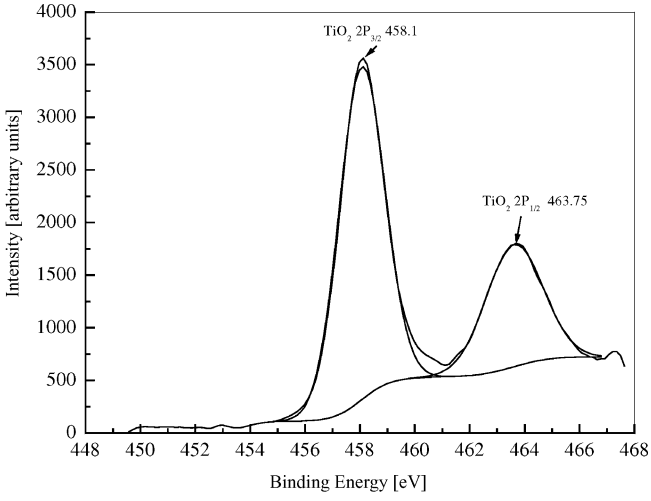

Figure 9. High-resolution XPS spectra of the 2p region of Ti in the TiO_2 sample doped with 1 atom-% Nb and Sc each.

Figure 10 shows the effect of doping on 2-chlorophenol photodegradation under visible light. The experiments carried out to examine the photodegradation of 2-chlorophenol under visible light indicate that the Sc and Nb codoped TiO_2 nanoparticles are relatively more photoactive with visible light than the particles doped with Nb or Sc alone. Furthermore, the Nb-doped samples show better photoactivity relative to the Sc-doped samples. Our results are consistent with those reported previously.[21,22] Cui et al.[21] reported that Nb doping in TiO_2 leads to enhanced photocatalytic activity in the destruction of many organic pollutants. Pep et al.[22] also reported a substantial increase in the photodegradation of 4-chlorophenol on TiO_2 film doped with Nb. New molecular orbitals are formed as a result of doping, which effectively narrow the bandgap. The effects of doping with metal ions such as Nb^{5+} and Sc^{3+} can be attributed to the introduction of new electronic states into the band structure of TiO_2, whose energies makes them accessible by photon excitation during the catalytic reaction.

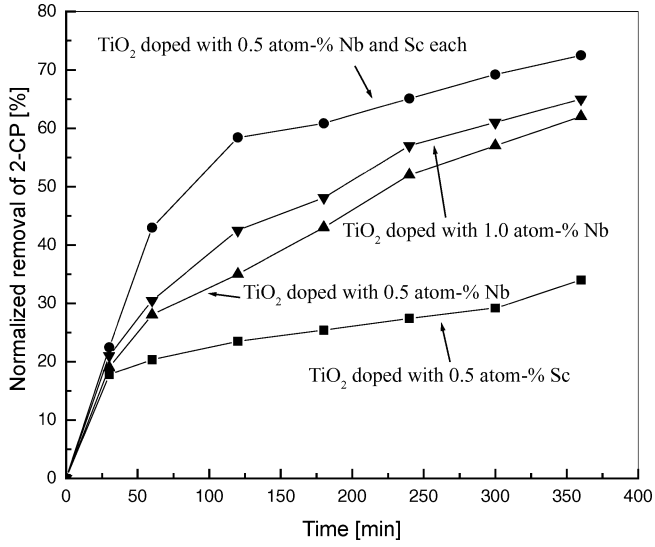

Figure 10. Effect of doping on 2-chlorophenol photodegradation under visible light.

Conclusions

We have synthesized TiO_2 nanoparticles by simultaneous doping with Nb and Sc through the sol–gel technique by using $TiCl_4$ as precursor. The as-prepared particles are amorphous in nature. The simultaneous doping of Nb and Sc has a significant effect on the transformation of anatase to the rutile phase. By increasing the Nb and Sc content from 0.5 atom-% each to 1.0 atom-% each, the anatase phase is stabilized. The XRD results indicate that the presence of Nb and Sc substitutional ions in the anatase crystal structure inhibits the phase transition and growth of the nanoparticles with an increase in temperature. When the calcination temperature is increased, the Nb and Sc ions are segregated out from the grains. As explained by Arbiol et al.,[13] at high temperatures, as soon as part of the added dopant is outside the anatase structure, the number of oxygen vacancies would be recovered in order to ensure crystal charge neutrality, and this would favor the anatase to rutile phase transition. The XPS results indicate the incorporation of Nb as Nb_2O_5 and Sc as Sc_2O_3. Additionally no metallic peaks were found within the XRD and XPS detection limits. Preliminary experiments carried out to examine the photodegradation of 2-chlorophenol under visible light indicate that the Sc and Nb codoped TiO_2 nanoparticles are relatively more photoactive with visible light than the particles doped with Nb or Sc alone.

Experimental Section

The sol–gel technique was used to synthesize doped titania nanoparticles. As mentioned earlier, this technique is capable of producing highly homogeneous doped and undoped metal oxide nanoparticles. For the synthesis, niobium pentaethoxide $Nb(OC_2H_5)_5$ was used as the Nb precursor and scandium acetylacetonate $Sc(CH_3COCHCOCH_3)_3$ was used as the Sc precursor, while titanium tetrachloride was used as the titanium dioxide precursor.

The doped titania nanoparticles containing 0.5, 0.75, and 1 atom-% Nb and Sc each were synthesized. The dopant stoichiometry was controlled by dissolving the Nb and Sc precursors in ethanol (Pharmco 200 proof) prior to the dropwise addition of $TiCl_4$. The reaction was performed at room temperature whilst stirring under a fume hood because of the large amount of Cl_2 and HCl gases evolved in this reaction. The resulting yellow solution was allowed to cool back to room temperature as gas evolution ceased. The suspensions obtained were dried in an oven for several hours at 60–80 °C until dried TiO_2 particles were obtained. The obtained Nb/Sc-doped samples were calcined for 1 h in a box furnace at temperatures ranging from 300–900 °C in an ambient atmosphere. XRD analysis of the doped and undoped TiO_2 powders was carried out on a Rigaku D-Max B diffractometer equipped with a graphite crystal monochromator, operating with a Cu anode and a sealed X-ray tube. The 2θ scans were recorded at several resolutions by using Cu-K_α radiation with a wavelength of 1.54 Å in the range 20–80° with a 0.05° step size. The recorded patterns were analyzed by using Jade® and origin software to determine the peak position, width and intensity. Full-width at half-maxima (FWHM) data was analyzed by Scherer's formula [Equation (1)] to determine the average particle size.

λ is the X-ray wavelength, β is the peak width, and θ is Bragg's angle. Since the peak width used in the Scherer's formula also includes the line broadening due to the strain in the particles, measurements of the particle size and distribution were also carried out by TEM. Both bright-field and dark-field micrographs were taken with a JEOL JEM-2000FX operating at 200 kV. The samples for TEM were prepared by dropping a dilute suspension of the sample powders onto a 300-mesh Lacy carbon grid. A dilute suspension was prepared by sonicating the particles in acetone for 5–10 min.

$$t = \frac{0.9\lambda}{\beta \mathrm{Cos}\theta} \quad (1)$$

XRD analysis was performed to determine the effect of the Nb/Sc doping on the rutile and anatase concentrations. For this, the mass fraction of rutile (X_r) in the samples calcined at various temperatures was calculated on the basis of the relationship between the integrated intensities of anatase (101) and rutile (110) peaks by the following formula [Equation (2)] developed by Spurr and Myers.[23]

I_a and I_r are the integrated peak intensities of the anatase and rutile peaks, respectively. The constant K was determined previously by

$$X_r = \frac{1}{(1 + KI_a / I_r)} \quad (2)$$

Burns et al.[6] and Barakat et al.[7] through an XRD analysis of a standard mixture of TiO_2 powder (Degussa P-25) of known proportions of anatase and rutile (80:20) and is equal to 0.79.

The dopant concentration was verified by EDS analysis and XPS. XPS was also employed to characterize the oxidation state of Nb and Sc in the doped samples. XPS was performed by irradiating the samples with monoenergetic soft X-rays and analyzing the energy of the electrons emitted. A SSI-M probe XPS was used that employed Al-K_α (hv = 1486.6 eV) exciting radiation. Peak positions were internally referenced to the C_{1s} peak at 284.6 eV. In addition to the survey scans, high-resolution scans in the Ti 2p, Nb 3d, Sc 2p, O 1s, and C 1s regions were also recorded. The Ti 2p, Nb 3d, and Sc 2p regions were used to determine the composition of the nanoparticles and to ascertain the valence states of Ti and the dopants.

Acknowledgments

Thanks are due to the Fulbright Scholarship Commission for provision of Fulbright postdoctoral fellowship to A. A.

[1] A. Sclafani, L. Palmisano, E. Davi, *J. Photochem. Photobiol.* **1991**, *A56*, 113–123.
[2] T. Sugimoto, X. Zhou, A. Muramatsu, *J. Colloid Interface Sci.* **2003**, *259*, 43–52.
[3] A. Fujishima, T. N. Rao, D. A. Tryk, *J. Photochem. Photobiol. C: Photochem. Rev.* **2000**, *1*, 1–21.
[4] H. E. Chao, Y. U. Yun, H. U. Xingfang, A. Larbot, *J. Eur. Ceram. Soc.* **2003**, *23*, 1457–1464.
[5] W. Li, Y. Wang, H. Lin, S. Ismat Shah, C. P. Huang, D. J. Doren, S. A. Rykov, J. G. Chen, M. A. Barteau, *Appl. Phys. Lett.* **2003**, *83*, 4143–4146.
[6] A. Burns, G. Hayes, W. Li, J. Hirvonen, J. D. Demaree, S. Ismat Shah, *Materials Science and Engineering B* **2004**, MSB 9793, 1–6.
[7] M. A. Barakat, G. Hayes, S. Ismat Shah, *J. Nanosci. Nanotechnol.* **2005**, *X*, 1–7.
[8] Y. Liu, C.-y. Liu, Q.-h. Rong, Z. Zhang, *Appl. Surf. Sci.* **2003**, *220*, 7–11.
[9] I. H. Teeng, W. C. Chang, J. C. S. Wu, *Appl. Catal., B* **2002**, *37*, 37–48.
[10] Z. H. Yuan, J. H. Jia, L. D. Zhang, *Mater. Chem. Phys.* **2002**, *73*, 323–326.
[11] H. Yamashita, M. Harada, J. Misaka, M. Takeuchi, K. Ikeue, M. Anpo, *J. Photochem. Photobiol.* **2002**, *148*, 257–261.
[12] M. A. Barakat, H. Schaeffer, G. Hayes, S. Ismat Shah, *Appl. Catal., B* **2004**, *57*, 23–30.
[13] J. Arbiol, J. Cerda, G. Dezanneau, A. Cirera, F. Peiro, A. Cornet, J. R. Mornate, *J. Appl. Phys.* **2002**, *92*, 853–861.
[14] A. Gribb, J. Banfield, *Am. Mineral.* **1997**, *82*, 717–728.
[15] D. R. Zhang, Y. H. Kim, Y. S. Kang, *J. Curr. Appl. Phys.* **2006**, *6*, 801–804.
[16] A. Ahmad, J. Thiel, S. Ismat Shah, *J. Phys.: Conf. Ser.* **2007**, *61*, 11–15.
[17] M. Sacerdoti, M. C. Dalconi, M. C. Carotta, B. Cavicchi, M. Ferroni, S. Colonna, M. L. Di Vona, *J. Solid State Chem.* **2004**, *177*, 1781–1788.
[18] D. Morris, Y. Dou, J. Rebane, C. E. J. Mitchell, R. G. Egdell, *Phys. Rev. B* **2000**, *61*, 13445–13457.
[19] F. M. F. de Groot, J. C. F. Fuggle, *Phys. Rev. B* **1990**, *41*, 928.
[20] A. Burns, W. Li, C. Baker, S. I. Shah, *Mater. Res. Soc. Symp. Proc.* **2002**, V. 5.2.1. 703.
[21] H. Cui, K. Dwight, S. Soled, A. Wold, *J. Solid State Chem.* **1995**, *115*, 187–192.
[22] C. Pepe, R. Amadelli, N. Pimpinelli, L. Cassar, Proceeding of the RILEM International Symposium on Environmental Conscious Materials and Systems for Sustainable Development, Koriyama, Japan, **2004**, 331–336.
[23] R. Spurr, H. Myers, *Anal. Chem.* **1957**, *29*, 760–762.

Received: September 19, 2007
Published Online: January 25, 2008

